Implementing Fast-Haar Wavelet transform on original Ikonos images to perform image fusion: qualitative assessment

Implementación de la Transformada Rápida de Haar con una imagen original Ikonos para la fusión de imágenes: evaluación cualitativa

Javier Medina[1-3]*, Carlos Pinilla[2] Luis Joyanes[3].

[1]Proyecto Curricular Ingeniería Catastral y Geodesia, Facultad de Ingeniería, Universidad Distrital Francisco José de Caldas (UDFJ). Bogotá DC., Colombia.

[2]Departamento de Ingeniería Cartográfica, Geodésica y Fotogrametría, Universidad de Jaén (UJA). Jaén, España

[3]Escuela Superior de Ingeniería y Arquitectura, Universidad Pontificia de Salamanca (UPSAM). Madrid, España.

Abstract

This article presents the Fast Haar Wavelet Transform (FHWT) algorithm applied to satellite-images fusion. FHWT is applied to both a multispectral image and a panchromatic Ikonos image using the digital image processing toolbox and wavelet toolbox provided by MatLab®. The results of the fusion are analyzed and evaluated quantitatively. Regarding the quantitative results of the fusion, first the mathematical-statistical correlation algorithm is used to analyze the spectral and spatial gain of the merged images. Next, the kappa coefficient is analyzed on three samples taken from the merged images, which are binarized in order to identify their spatial accuracy. It is shown that FHWT outperforms other predefined wavelets (namely rbio6.8, bior6.8, db7, dmey and haar) when merging the images. Moreover, merged images maintain the same spectral output as the original image, and also exhibit significant spatial resolution gain.

---

* Autor de correspondencia: teléfono: + 57 + 1 + 703 44 44, correo electrónico: rmedina@udistrital.edu.co (J Medina)

Resumen

Este artículo presenta la transformada rápida de Wavelet Haar (FHWT, de la sigla en inglés) algoritmo que se aplica a la fusión de imágenes satelitales. FHWT es aplicado en un par de imágenes, una imagen multiespectral y una imagen pancromática Ikonos, usando el toolbox de procesamiento digital de imágenes y el toolbox de wavelet suministrados por MatLab®. Los resultados de la fusión son analizados y evaluados cuantitativa. En lo que corresponde a los resultados cuantitativos de la fusión, se utilizan, en primer lugar, el algoritmo de correlación matemática estadística para analizar la ganancia espectral y espacial de las imágenes fusionadas. Posteriormente, tres sub-imágenes de las imágenes fusionadas son binarizadas con el fin de identificar su precisión espacial, y son evaluadas a través del coeficiente kappa. Los resultados demuestran que FHWT supera a las otras wavelets estudiadas (rbio6.8, bior6.8, db7, dmey y haar) al fusionar las imágenes. Por otra parte, las imágenes fusionadas con la FHWT mantienen la resolución espectral respecto a la imagen multiespectral original, mientras presentan una ganancia importante en la resolución espacial.

----------Palabras clave: Transformada Wavelet, fusión de imágenes, transformada rápida de Wavelet Haar (FHWT), transformación RGB-IHS, algoritmo de Mallat, imágenes del IKONOS

Introduction

The main purpose of using digital techniques is to process an image in such a way that the resulting data-image is more suitable for a specific application than the original image. To do so, digital image processing focuses on achieving three basic principles, namely correcting the image data, enhancing the original image, and classifying (or extracting) image data [1, 2]. Most of the time, the image data provided by the agencies is corrected geometrically and radiometrically. However, some processes require raw data, and when that is the case, users are in charge of dealing with these corrections [3, 4].

Image fusion allows the combination and utilization of image data coming from different sources with different degrees of spatial resolution. The point is to obtain "higher-quality" information; the exact definition of "higher quality" depends on the application [5, 6]. Conventional procedures for merging images are based on different techniques, such as RGB-to-HIS transformation, Brovey transform, and the method of principal components, among others. These methods are not entirely satisfactory because they degrade spectral information. In recent years, image-merging techniques have begun to include procedures that use two-dimensional wavelet transforms, preserving the spectral richness of the original images up to a great extent [7 - 10]. The image fusion techniques that rely on wavelets as an alternative solution can be used to integrate the geometric details of a high-resolution panchromatic image (PAN), and also to integrate the colour of a multispectral image (MS) with low spatial resolution; the result is a new multispectral image (N-MS) with high spatial resolution and proper preservation of spectral richness [11, 12]. These results satisfy the frequent need of users to have a single set of image data that include high spectral and spatial resolution from both multispectral images and panchromatic images, particularly when such images have different spatial resolutions and come from different remote sensors. This type of fusion allows having detailed information on urban and rural environments [13], which is useful for applications such as

urban planning and management. Additionally, image fusion is widely used in the development of projects in various fields such as agriculture, hydrology, the environment, and natural-disaster monitoring services, among others.

The present paper focuses on implementing the fast Haar wavelet transform (FHWT) for the fusion of satellite images. Such an implementation involved the use of an Ikonos multispectral image together with an Ikonos panchromatic image, and also MatLab as the chosen software package. The first part of the paper is a review of two mathematical concepts necessary to carry out a 2-D decomposition the fast Haar wavelet transform FHWT in this implementation, namely RGB to IHS transform, Mallat's algorithm. Then, in order to evaluate the effectiveness of FHWT when fusing images, we compared an Ikonos image merged through FHWT, with the same image merged by using five wavelets predefined in MatLab®, namely bior 6.8, rbio6.8, db7, dmey, and haar. Throughout the paper, FHWT performance is compared to others five wavelets, which were implemented for image merging and were generated using the wavelet toolbox and image processing toolbox of MatLab [14, 15]. Finally, the results of the six merged images are presented and assessed quantitatively with respect to two indexes. The first index is a mathematical-statistical result obtained from the spatial and spectral correlation coefficients of the original images when compared to the merged images. The second index is the calculation of the kappa coefficient together with the overall accuracy of three sample sub-images, which were binarized as a result of the extraction of urban objects found in these sub-images. The results of such analysis and the conclusions are presented at the end of the paper.

Mathematical concepts to carry out a 2-d decomposition the Fast Haar

IHS model transformation

The colours in the IHS model are defined with respect to the normalized values of red, green and blue, given in terms of RGB colours by primary (equations 1-3):

$$r = \frac{R}{(R + G + B)} \qquad (1)$$

$$g = \frac{G}{(R + G + B)} \qquad (2)$$

$$b = \frac{B}{(R + G + B)} \qquad (3)$$

Where R, G and B have been normalized so that they are in the interval [0,1], the equations (1)-(3) show that, and also belongs to the interval [0,1] and that (equation 4):

$$r + g + b = 1 \qquad (4)$$

Normalized changes have to satisfy equation (4) [4]. For three arbitrary colour components R, G and B, all of them in the interval [0,1], the intensity component in the IHS model is defined in the equation (5) as:

$$I = \frac{1}{3}(R + G + B) \qquad (5)$$

The equation (6) for H in terms of, G, and B

$$H = \arccos\left(\frac{\frac{1}{2}[(R - G) + (R - B)]}{[(R - G)^2 + (R - B)(G - B)]^{\frac{1}{2}}}\right) \qquad (6)$$

Saturation according (equation 7) to the set of values R, G and B primary:

$$S = 1 - \left(\frac{3}{(R + G + B)}\right)[\min(R, G, B)] \qquad (7)$$

The Mallat's algorithm

In order to understand the multiresolution analysis concept based on Mallat's algorithm it is very useful to represent the wavelet transform as a pyramid. The basis of the pyramid is the original image, with C columns and R rows. Each level of the pyramid, which is only accessible from the immediately lower level, is an approximation to the original image. When climbing up in the pyramid, the successive approximation images have a coarser spatial resolution. At the *Nth* level,

the approximation image has $C/2^N$ columns and $R/2^N$ rows because a dyadic wavelet transform with subsampling or decimation is applied [16].

These approximation images are computed using scaling functions related to the Mother Wavelet function $P(x)$ [16, 17]. The difference between the information from two successive levels of the pyramid, e.g. between the original image A_2^j at a resolution 2^j and the approximation image A_2^{j-1} at a resolution 2^{j-1} is given by the wavelet transform, and computed using the wavelet functions. Three wavelet coefficient images, H_2^{j-1}, V_2^{j-1} and D_2^{j-1} pick up, respectively, the horizontal, vertical and diagonal detail that is lost between the images A_2^j and contain the features with sizes comprised between 2^j and 2^{j-1} resolution (non-redundant DWT algorithm). If the original image has C columns and R rows, the approximation and the wavelet coefficient images obtained applying this multiresolution decomposition have $C/2$ columns and $R/2$ rows. When the inverse wavelet transform is applied, the original image A_2^j can be reconstructed exactly from the approximation image A_2^{j-1} and the horizontal, vertical and diagonal wavelet coefficients H_2^{j-1}, V_2^{j-1} and D_2^{j-1}. For the practical implementation of Mallat's algorithm, quadrature mirror filters are used instead of the scaling and wavelet functions. The 'h' filter, associated with the scaling function, is a one-dimensional low pass filter that allows the analysis of low frequency data, while the 'g' filter, associated with the wavelet function, is a one-dimensional high pass filter that allows the analysis of the high frequency components, i.e. the detail of the image being analysed [18]. The number of parameters of these filters and the value of these parameters depend on the Mother Wavelet function used in this analysis. In this work, we use the FWTH.

Two-dimensional Haar Wavelet

The basic two-dimensional Haar Wavelet transforms

Let f be a function approximated by a square-step function $\vec{f}$ and encoded by a matrix [19].

$$\vec{f} = \begin{pmatrix} f(0,0) & f\left(0,\dfrac{1}{2}\right) \\ f\left(\dfrac{1}{2},0\right) & f\left(\dfrac{1}{2},\dfrac{1}{2}\right) \end{pmatrix} = \begin{pmatrix} S_{0,0} & S_{0,1} \\ S_{1,0} & S_{1,1} \end{pmatrix}$$

The matrix above encodes the values of f, but for some applications, change patterns prove more useful than the values themselves. One method to calculate such patterns expresses the same function in terms of two-dimensional wavelets [17, 20]. For instance, one algorithm begins with a one-dimensional wavelet transform of each row,

$$\begin{pmatrix} S_{0,0} & S_{0,1} \\ S_{1,0} & S_{1,1} \end{pmatrix} \rightarrow \begin{pmatrix} \dfrac{S_{0,0} + S_{1,0}}{2} & \dfrac{S_{0,0} - S_{0,1}}{2} \\ \dfrac{S_{1,0} + S_{1,1}}{2} & \dfrac{S_{1,0} - S_{1,1}}{2} \end{pmatrix}$$

And then a one-dimensional wavelet transforms for each new column,

$$\begin{pmatrix} \dfrac{S_{0,0} + S_{1,0}}{2} & \dfrac{S_{0,0} - S_{0,1}}{2} \\ \dfrac{S_{1,0} + S_{1,1}}{2} & \dfrac{S_{1,0} - S_{1,1}}{2} \end{pmatrix}$$

$$\downarrow$$

$$\begin{pmatrix} \dfrac{(S_{0,0} + S_{1,0}) + (S_{1,0} + S_{1,1})}{2} & \dfrac{(S_{0,0} - S_{0,1}) + (S_{1,0} - S_{1,1})}{2} \\ \dfrac{(S_{0,0} + S_{1,0}) - (S_{1,0} + S_{1,1})}{2} & \dfrac{(S_{0,0} - S_{0,1}) - (S_{1,0} - S_{1,1})}{2} \end{pmatrix}$$

Two dimensional Fast Haar Wavelet Transform

The one-dimensional fast wavelet transform extends to a two-dimensional fast wavelet transform with tensor product by alternately applying the one-dimensional transform to each row and then to each new column.

Consider a function $\vec{f}$ sampled at values on a square grid, and approximated by corresponding square-step function.

$$\vec{f} = \begin{pmatrix} a_{11} & a_{12} & a_{13} & a_{14} \\ a_{21} & a_{22} & a_{23} & a_{24} \\ a_{31} & a_{32} & a_{33} & a_{34} \\ a_{41} & a_{42} & a_{43} & a_{44} \end{pmatrix}$$

The first step, namely the two-dimensional transform, consists of a first one-dimensional step for each row

$$
\begin{pmatrix}
a_{11} & a_{12} & a_{13} & a_{14} \\
a_{21} & a_{22} & a_{23} & a_{24} \\
a_{31} & a_{32} & a_{33} & a_{34} \\
a_{41} & a_{42} & a_{43} & a_{44}
\end{pmatrix}
\rightarrow
\begin{pmatrix}
\dfrac{a_{11}+a_{12}}{2} & \dfrac{a_{11}-a_{11}}{2} & \dfrac{a_{13}+a_{14}}{2} & \dfrac{a_{13}-a_{14}}{2} \\
\dfrac{a_{21}+a_{22}}{2} & \dfrac{a_{21}-a_{22}}{2} & \dfrac{a_{23}+a_{24}}{2} & \dfrac{a_{23}-a_{24}}{2} \\
\dfrac{a_{31}+a_{32}}{2} & \dfrac{a_{31}-a_{32}}{2} & \dfrac{a_{33}+a_{34}}{2} & \dfrac{a_{33}-a_{34}}{2} \\
\dfrac{a_{41}+a_{42}}{2} & \dfrac{a_{41}-a_{42}}{2} & \dfrac{a_{43}+a_{44}}{2} & \dfrac{a_{43}-a_{44}}{2}
\end{pmatrix}
=
\begin{pmatrix}
c_{11} & c_{12} & c_{13} & c_{14} \\
c_{21} & c_{22} & c_{23} & c_{24} \\
c_{31} & c_{32} & c_{33} & c_{34} \\
c_{41} & c_{42} & c_{43} & c_{44}
\end{pmatrix}
$$

followed by a first one-dimensional step for each new column

$$
\begin{pmatrix}
c_{11} & c_{12} & c_{13} & c_{14} \\
c_{21} & c_{22} & c_{23} & c_{24} \\
c_{31} & c_{32} & c_{33} & c_{34} \\
c_{41} & c_{42} & c_{43} & c_{44}
\end{pmatrix}
$$

$$\downarrow$$

$$
\begin{pmatrix}
\dfrac{c_{11}+c_{21}}{2} & \dfrac{c_{12}+c_{22}}{2} & \dfrac{c_{13}+c_{23}}{2} & \dfrac{c_{14}+c_{24}}{2} \\
\dfrac{c_{11}-c_{21}}{2} & \dfrac{c_{12}-c_{22}}{2} & \dfrac{c_{13}-c_{23}}{2} & \dfrac{c_{14}-c_{24}}{2} \\
\dfrac{c_{31}+c_{41}}{2} & \dfrac{c_{32}+c_{42}}{2} & \dfrac{c_{33}+c_{43}}{2} & \dfrac{c_{34}+c_{44}}{2} \\
\dfrac{c_{31}-a_{41}}{2} & \dfrac{c_{32}-c_{42}}{2} & \dfrac{c_{33}-c_{43}}{2} & \dfrac{c_{33}-c_{44}}{2}
\end{pmatrix}
=
\begin{pmatrix}
d_{11} & d_{12} & d_{13} & d_{14} \\
d_{21} & d_{22} & d_{23} & d_{24} \\
d_{31} & d_{32} & d_{33} & d_{34} \\
d_{41} & d_{42} & d_{43} & d_{44}
\end{pmatrix}
$$

The intermediate result obtained above corresponds to one basic two-dimensional wavelet transform on each of the four adjacent 2×2 squares. Then, method available to complete the two-dimensional transform, as done here [20]. Before proceeding to explain the second two-dimensional step, it is convenient to rewrite the intermediate result just obtained so as to group similar wavelets together:

$\begin{pmatrix} A \\ \\ \end{pmatrix}$ All the sums from the upper left-hand corners of the four 2×2 blocks go into the upper left-hand corner of the grid.

$\begin{pmatrix} & h \\ & \end{pmatrix}$ All the differences from the upper right-hand corners of the four 2×2 blocks go into the upper right-hand corner of the large grid.

$\begin{pmatrix} \\ v \end{pmatrix}$ All the differences from the lower right-hand corners of the four 2×2 blocks go into the lower right-hand corner of the large grid.

$\begin{pmatrix} \\ & d \end{pmatrix}$ All the differences from the lower left-hand corners of the four 2×2 blocks go into the lower left-hand corner of the large grid.

$$
\begin{pmatrix}
d_{11} & d_{12} & d_{13} & d_{14} \\
d_{21} & d_{22} & d_{23} & d_{24} \\
d_{31} & d_{32} & d_{33} & d_{34} \\
d_{41} & d_{42} & d_{43} & d_{44}
\end{pmatrix}
\rightarrow
\begin{pmatrix}
d_{11} & d_{13} & d_{12} & d_{14} \\
d_{31} & d_{33} & d_{32} & d_{34} \\
d_{21} & d_{23} & d_{22} & d_{24} \\
d_{41} & d_{43} & d_{42} & d_{44}
\end{pmatrix}
$$

Finally, a two-dimensional wavelet transform is performed only on the four entries in the upper left-hand corner:

$$A = \begin{pmatrix} d_{11} & d_{13} \\ d_{31} & d_{33} \end{pmatrix} \xrightarrow{\rightarrow} \begin{pmatrix} \dfrac{d_{11} + d_{13}}{2} & \dfrac{d_{11} - d_{13}}{2} \\ \dfrac{d_{31} + d_{33}}{2} & \dfrac{d_{31} - d_{33}}{2} \end{pmatrix} = \begin{pmatrix} b_{11} & b_{21} \\ b_{21} & b_{22} \end{pmatrix}$$

$$\downarrow$$

$$\begin{pmatrix} \dfrac{b_{11} + b_{13}}{2} & \dfrac{b_{21} + b_{22}}{2} \\ \dfrac{b_{11} - b_{21}}{2} & \dfrac{b_{21} - b_{22}}{2} \end{pmatrix} = \begin{pmatrix} A1 & H2 \\ V2 & D2 \end{pmatrix} = A2c$$

Thus the complete two-dimensional wavelet transform emerges:

$$\begin{pmatrix} A2 & H2 & d_{12} & d_{14} \\ V2 & D2 & d_{32} & d_{34} \\ d_{21} & d_{23} & d_{22} & d_{24} \\ d_{41} & d_{43} & d_{42} & d_{44} \end{pmatrix}$$

where, $h = H1 = \begin{pmatrix} d_{12} & d_{14} \\ d_{32} & d_{34} \end{pmatrix}$, $d = D1 = \begin{pmatrix} d_{22} & d_{24} \\ d_{42} & d_{44} \end{pmatrix}$ and

$v = V1 = \begin{pmatrix} d_{21} & d_{23} \\ d_{41} & d_{43} \end{pmatrix}$, the completed two-dimensional wavelet transform is then:

$$\begin{pmatrix} A2c & H1 \\ V1 & D1 \end{pmatrix}$$

Material and methods

Study area

The study area is located in Bogotá D.C. (Colombia), specifically in a Metropolitan Park called "Parque Simón Bolívar", which is captured by an Ikonos image. The sub-image Ikonos panchromatic band has a 1-meter spatial resolution (Figure 1a) and the Ikonos multispectral image has three multispectral channels (R-red G-green B-blue) with a spatial resolution of 4 meters (Figure 1b). The images were acquired on September 6th 2007, their reference system is UTM / WGS 84. The two images were cut out at 2048x2048 pixels in order to satisfy Dyadic's characteristic [10].
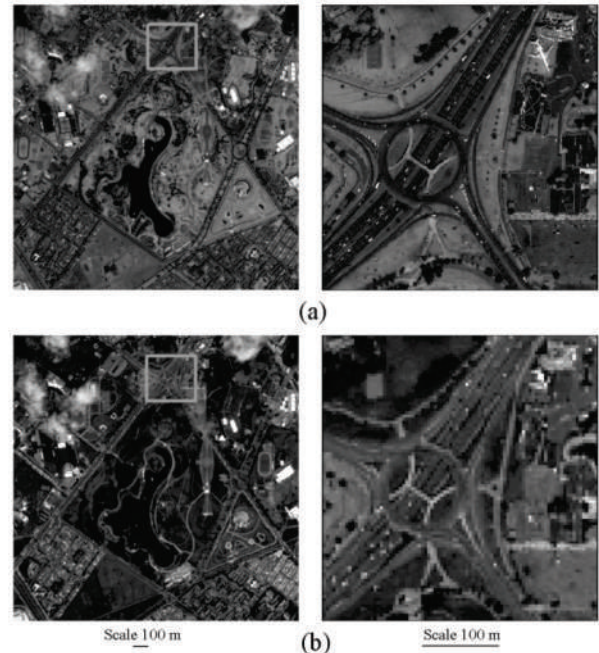

Figure 1 (a) Ikonos panchromatic image. (b) Ikonos multispectral image true colour composition

77

Methodology

Five major stages were completed in order to achieve the fusion of satellite images and also to analyze the results.

The first stage corresponded to image pre-processing; this stage included the acquisition of multispectral and panchromatic Ikonos images, the analysis of existing information about the study area (Simón Bolívar Park located in Bogotá D.C. - Colombia), the calculation of the basic statistics, image corrections, image enhancements and geo-referencing, and the cropping as well as re-sampling of images.

The second stage dealt with the implementation of the Fast Haar Wavelet Transform FHWT, which is the main focus of this study. Also included in this stage was the generation of a fusion image using the FHTW, which involved the use of MatLab.

The third stage concerned the generation of a five-image merge using five wavelets, also implemented in MatLab [14].

The fourth stage evaluated the merged images according to the three indexes: a) correlation coefficient, b) kappa coefficient of binary images, and c) information gathering through expert-panel questionnaire to identify the best merged image.

The fifth and final stage produced the result analysis and the concluding remarks.

Implementation two-dimensional Fast Haar Wavelet transform in image fusion

Based on the mathematical algorithm previously described [19], and as a result of this research, we propose the following steps (based on the RGB-IHS transform) and the pyramidal algorithm to implement the FHWT transform and merge satellite images [16, 21]:

Implementation of the Fast Haar Wavelet Transform, based on the mathematical algorithm described previously §2, and also as a result of this research, we propose the following steps (figure 2) to implement the FHWT for merging satellite images:

1) Make an RGB colour composition of the multispectral image (MUL) [4, 22]. In this case study, two colour compositions were used, namely a true-colour composition (RGB) and a false-colour composition (NIRBR). The following steps are carried out independently for each one of the compositions.

2) Resample the colour composition at the same pixel size as that of the panchromatic image.

3) Transform RGB components into intensity-hue-saturation (IHS) components.

4) Apply FHWT to component I. For this application, it is necessary to know the decomposition level of the image on which fusion is performed. For instance, given that the panchromatic IKONOS image has a spatial resolution of 1 meter and the multispectral IKONOS image has a spatial resolution of 4 meters, the following calculation can be used: $\frac{4}{1} = 4$. On the other hand, given the 2^n relationship of dyadic characteristic, it is true that $n=2$ fulfill this condition because $2^2=4$. For this reason 2 should be selected as a suitable decomposition level. Therefore, the FHWT must be applied iteratively up to the second decomposition level of component I (intensity) so as to obtain the approximation coefficients and the detail coefficients. Matrix A1i holds the approximation coefficients of intensity component I. Similarly, matrices V1i, D1i and H1i store the detail coefficients of I. Next, A1i is decomposed a second time to obtain A2i, V2i, H2i and D2i, where A2i holds the approximation coefficients of the second decomposition level of I. Likewise, the detail coefficients of this second-level decomposition of I are stored in V2i, H2i, and D2i.

5) Apply the concept of FHWT to the panchromatic image (PAN). Just like in the

case of intensity component I, FHWT is applied iteratively until the second PAN decomposition level is obtained, which allows extracting the approximation coefficients and detail coefficients. Matrix A1p holds approximation coefficient of PAN. Matrices V1p, H1p and D1p keep the detail coefficients of PAN. Next, A1p is decomposed a second time to obtain the approximation coefficients (A2p) of PAN. The detail coefficients of the second decomposition level of PAN are then V2p, H2p, and D2p.

6) Generate a new intensity component (N-INT). The new component N-INT is the concatenation of the approximation coefficients of I and the detail coefficients of PAN. This is obtained by using the second-level approximation coefficients of I (A2i), the second-level detail coefficients of PAN (V2p, H2p and D2p), and also the first-level detail coefficients of PAN (V1p, H1p and D1p).

7) Apply the inverse transform of the Fast Haar Wavelet Transform (I-FHWT) to obtain the new intensity component NI.

8) Make a colour composition based on the NI and the original hue and saturation components in order to generate the new NI-HS.

9) Perform IHS-to-RGB transformation on the newly found NI-HS components in order to obtain a new multispectral N-RGB image from the true colour composition, and also an N-NIRBR image from the false colour composition, which largely keep the spectral resolution of the original multispectral images and further provide greater spatial resolution.

10) Through layer-stack, take the new RGB fused channels from the true-colour composition and the new NIR fused channel from the false-colour composition so as to obtain a complete four-channel fused image.
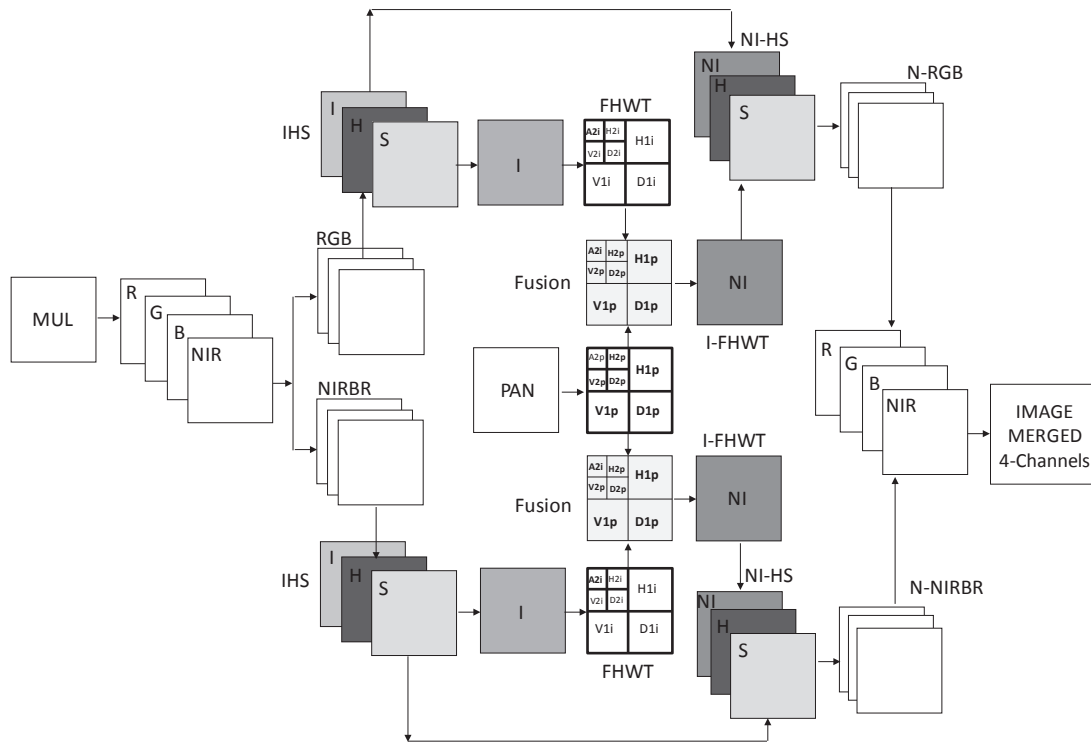

Figure 2 Workflow processes to obtain a merged image using FHWT

The net result is a four-channel image that exhibits the spectral resolution from the original multispectral image while bearing the spatial resolution from the original panchromatic image.

Fusion satellite images using other wavelet transforms

In order to validate the proposed method that implements FHWT, the same process-flow was implemented using other five wavelets, namely bior6.8, rbio6.8, db7, dmey, and haar. These wavelets were selected due to their remarkable performance within a larger group of wavelets [23, 24]. Both the digital image processing toolbox [14] and wavelet toolbox of Matlab were used for the fusion of satellite images [15]. Regarding the process itself, the only difference lay in the use of each selected wavelet for decomposing both component I and the panchromatic image instead of using the proposed FHWT.

Results

For the evaluation and analysis of the results obtained after merging the images by means of the two procedures mentioned above, the two methods described below were considered:

Quantitative results using a mathematical-statistical method

To analyze spectral-resolution conservation after the fusion process in the two cases (i.e. images merged with the transform FHWT as well as those merged with the 5 wavelets), the correlation between each of these images and the original multispectral image was calculated.

Regarding the degree of spatial-resolution conservation, for each band of the six merged images correlation was calculated with the original panchromatic image. This calculation was based on the following correlation formula (equation 8):

$$corr(A/B) = \frac{\sum_{j=1}^{\mathrm{npix}}(A_j - \overline{A})(B_j - \overline{B})}{\sqrt{\sum_{j=1}^{\mathrm{npix}}(A_j - \overline{A})\sum_{j=1}^{\mathrm{npix}}(B_j - \overline{B})}}$$

Where $\overline{A}$ and $\overline{B}$ represent the average values of the corresponding images, $corr(A/B)$ is the correlation coefficient and its range varies between -1 and $+1$. The signs $+$ and $-$ are used for positive and negative correlations, respectively. Note that $corr(A/B)$ is a dimensionless quantity, that is, it does not depend on the units [10, 11, 25].

The spectral correlation between each of the bands from the merged images (namely the images produced through FHWT, bior6.8, rbio6.8, db7, haar, and dmey) and each band from the multispectral original image (RGB) are shown in table 1.

Table 1 Comparison of Spectral Correlation Between the Multi-spectral Original image And Each Of the Six Merged Images

Images	R	G	B
RGB/FHWT	0.90	0.88	0.91
RGB/ bior6.8	0.90	0.85	0.90
RGB/rbio6.8	0.90	0.85	0.89
RGB/db7	0.89	0.84	0.89
RGB/haar	0.88	0.88	0.87
RGB/dmey	0.90	0.86	0.90

The spatial correlation between each of the bands from the merged images (FHWT, bior6.8, rbio6.8, db7, haar, and dmey) and the panchromatic original image (PAN) are shown in Table 2.

Table 2 Comparison of Spatial Correlation Between the Panchromatic Original Image and Each Of the Six Merged Images

Images	R	G	B
PAN/FHWT	0.60	0.67	0.54
PAN/ bior6.8	0.47	0.63	0.35
PAN/rbio6.8	0.50	0.65	0.40
PAN/db7	0.50	0.65	0.39
PAN/haar	0.51	0.66	0.39
PAN/dmey	0.50	0.65	0.39

Quantitative results using a binarization method

Image binarization is a process where reduction of the same information takes place. In this process, only two values occur, namely true or false. In a digital image, these values (i.e. true and false) can be represented by the values 0 and 1 or, more commonly, by the colours black (gray value 0) and white (gray value 255). In processing and analyzing an image, binarization is used to separate objects of interest from other objects within an image, thus objects extracted from the merged images can be assessed. In this study, a technique based on Otsu's threshold algorithm was used [26]. Threshold is one of the most commonly used methods for image segmentation [27]. In this method, by selecting an adequate Threshold value T, gray-scale images can be converted into binary images. The resulting binary image should contain all the essential information about the position and shape of the objects of interest (foreground). The advantage of having a binary image is that it reduces data complexity and simplifies the process of recognition and classification. The problem of segmentation lies in selecting an appropriate value for the Threshold (T) because, in real applications, histograms are complex and so it is not always easy to select this value. For this study, object segmentation was carried out using the software package called Aphelion. This tool was applied to three sample sub-images, which were binarized for the purpose of evaluating the spatial accuracy of the merged images. Samples 1 and 2 correspond to airplanes, and sample 3 is a library building, hereinafter referred to as Sample 1, Sample 2 and Sample 3. To verify accuracy, the objects extracted from the original panchromatic image were compared with the objects extracted from each one of the merged images (Figure 3). Taking into account that binarization was carried out over a gray-scale image, then a "false panchromatic" was created from the average of the four bands (equation 9):

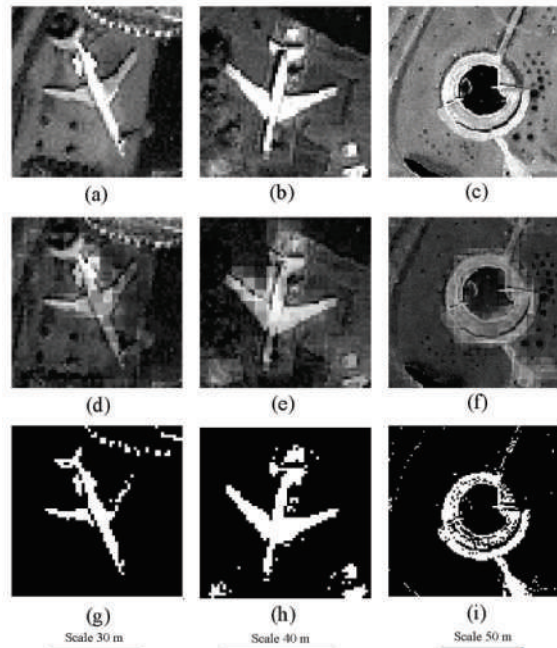$$FPAN = \frac{B + G + R + NIR}{4} \qquad (9)$$

Figure 3 Original panchromatic image. (a) sample 1. (b) sample 2. (c) sample 3, "False panchromatic" from the FHWT (d) sample 1. (e) sample 2. (f) sample 3. Images binarized from original panchromatic image (g) sample 1, (h) sample 2. (i) sample 3.

This was performed for each of the six merged images. The Kappa coefficient and the overall accuracy are calculated from the confusion matrices created for each of the comparisons. Cohen's kappa coefficient is a statistical measure of inter-rater agreement [28].

This coefficient measures the agreement between two raters, each classifying N items into C mutually exclusive categories. The equation (10) for k is the following:

$$k = \frac{Pr(a) - Pr(e)}{1 - Pr(a)} \qquad (10$$

where $P(a)$ is the relative agreement observed across raters, and $P(e)$ is the hypothetical probability of chance agreement, using the observed data to calculate the probabilities of each observer randomly. If the raters are in complete agreement, then k=1. If there is no agreement

81

across raters, other than what would be expected by chance, as indicated by $P(e)$, then $k=0$.

Both the Kappa coefficient and the percentage of overall accuracy obtained with the binarization method, when applied to the three sample images, are shown in Table 3.

Table 3 Comparison of Accuracy For Identification Objects ("Object-Oriented Classification") On Each Of The Three Sample images Merged With The Six Methods in Terms of Kappa Coefficients and Overall Accuracy (OA)

Image Fusion	Sample 1		Sample 2		Sample 3	
	K	OA (%)	K	OA (%)	K	OA (%)
FHWT	0.61	91.31	0.77	93.79	0.74	93.61
bior6.8	0.52	89.28	0.69	91.41	0.67	90.50
rbio6.8	0.51	89.31	0.68	91.52	0.61	88.41
db7	0.55	90.27	0.70	91.66	0.62	88.66
Dmey	0.59	91.29	0.70	91.81	0.63	88.31
Haar	0.57	90.78	0.76	93.62	0.61	88.36

Discussion

In order to validate the image fusion process conducted through six different methods (five wavelets available in MatLab, and the FHWT implemented by us); results were compared across two different indices. The first index was the correlation coefficient between merged images and original images; the second index concerns the binarization of objects. Regarding the two indicators, the FHWT showed the best results, indicating that FHWT actually improves the spatial resolution and also keeps the spectral resolution of the multispectral image.

As for the correlation coefficient of the multispectral image and the merged image, the highest value was 0.91 for the blue band; this value was obtained using FHWT. Regarding the green band, the highest value was 0.88, achieved by means of FHWT and the haar Transform. When considering the red band, all values remained

fairly homogeneous, ranging from 0.88 to 0.90. In this latter case, haar-associated values were the lowest (0.88). The value obtained by means of FHWT in the red band was 0.90. Regarding the correlation between the panchromatic image and each of the bands from the merged images, FHWT yielded the highest values in the three bands (R: 0. 60 – G: 0.67 – B: 0.54) when compared to the other wavelet methods in this study. With respect to the kappa coefficients of the three sample images, in general, the best coefficients for merged images were obtained through the FHWT method, showing substantial agreement. As for the Sample 1 (Airplane 1), overall accuracy fluctuated between 89.28% and 91.31%, and the highest level was obtained with FHWT. In Sample 2 (Airplane 2), accuracy levels ranged from 91.41% to 93.79%; where the highest accuracy level was obtained by means of FHWT and the second best performance was obtained from haar. When observing Sample 3 (library building), accuracy levels fluctuated between 88.31% and 93.41%; once again the highest value corresponds to that obtained with FHWT. These results further confirm the capabilities of the FHWT-associated fusion to maintain spectral resolution while improving spatial resolution. Additionally, the object-extraction method allowed evaluating the details of the image [5]. Thus, linear details (aircraft, highways, and buildings), texture (vegetation, trees) and colour (roofs of buildings, road surfaces, and grasslands) were also analyzed.

Conclusion

Previous studies have shown that image-fusion methods (merging) based on wavelet transform are more suitable for image fusion than conventional methods [7, 29]. Nevertheless, the method presented in this article, based on the fast haar transform wavelet (FHWT), which is fast, real and orthogonal, yielded better results than the other methods considered in this study through their properties are advantages for images processing, particularly in image fusion. The FHWT-associated method presented consists

in transforming an RGB colour composition into an IHS composition; then Intensity component coefficients (A2i) are extracted, capturing the spectral richness extracted from a multi-spectral image that has low resolution. Afterwards, a new intensity (NI) is generated as result of combining these coefficients (A2i) with the detail coefficients H2p, V2p, D2p, H1p, D1p, and so V1p is calculated from the panchromatic image that contains the spatial richness (intensity). Finally, the NI-HS colour composition is transformed into N-RGB colour composition, thus generating a merged image. The presented FHWT method is capable of improving the spatial quality of the multispectral image while preserving its spectral content as much as possible. In this study FHWT was implemented in MatLab, using an Ikonos multispectral image (4m spatial resolution) and an Ikonos panchromatic image (1m spatial resolution) of an area called "Parque Simón Bolívar" in Bogotá (Colombia). This FHWT method might be considered as an improvement because the intensity component is not totally replaced by the panchromatic image. The high spatial resolution of the panchromatic image is included in the intensity component by means of panchromatic wavelet-coefficient substitution for the intensity component. Finally, the benefits of using the proposed FHWT method, compared to using the other wavelet families, were evaluated qualitatively. In all cases, the values obtained through FHWT outperformed those obtained through implementation of the other five wavelet transforms tested in this study. The method achieves improvement of multi-spectral image spatial quality and further preserves spectral quality, which represents the attainment of the objectives set at the beginning of the whole research process presented herein.

Acknowledgements

References

1. E. Chuvieco. *Teledetección Ambiental*. 3ª ed. Ed. Arial S. A. 1996. Barcelona, España. pp.1-568.

2. C. Pinilla. *Elementos de Teledetección*. 1ª ed. Ed. Ra-Ma. Madrid, España. 1995. pp. 313.

3. K. Castleman. *Digital Image Processing*. 3ª ed. Ed. Prentice-Hall. 1979. Nueva Jersey. USA. pp. 1- 651.

4. R. González, R. Woods. *Tratamiento Digital de Imágenes*. 1ª ed. Ed. Diaz de Santos S. A. Wilmington, Estados Unidos. 1996. pp. 1-773.

5. L. Alparone, L. Wald, J. Chanussot, C. Thomas, P. Gamba, L. Bruce. "Comparison of Pansharpening Algorithms: Outcome of the 2006 GRS-S Data Fusion Contest". *IEEE Transactions on Geoscience and Remote Sensing*. Vol. 45. 2007. pp. 3012-3021.

5. C. Pohl, J. Van Genderen. "Multisensor Image Fusion in Remote Sensing: Concepts, Methods and Applications". *International Journal of Remote Sensing*. Vol. 19. 1998. pp. 823-854.

6. M. Gónzalez, R. García, J. Herrero. "Fusion of Multispectral and Panchromatic Images New Methods Based on Wavelet Transforms – Evaluation of Crop Classification Accuracy". T. Benes (editor). *Geoinformation for European-wide Integration*. 1ª ed. Ed. Millpress. Rotterdam, Netherlands. 2003. pp. 265-272.

7. M. Gónzalez, J. Saleta, R. García-C., R. García. "Fusion of Multispectral and Panchromatic Images Using Improved IHS and PCA Merges Based on Wavelet Decomposition". *International Journal of Remote Sensing*. Vol. 26. 2005. pp. 595-614.

8. C. Gonzalo, M. Lillo. "Fusión de Imágenes QuickBird Mediante una Representación Conjunta Multirresolución–Multidireccional". *IEEE Latin America Transactions*. Vol. 5. 2007. pp. 32-37.

9. J. Nuñez, X. Otazu, O. Fors, A. Prades, V. Pala, R. Arbiol. "Multiresolution-Based Image Fusion With Additive Wavelet Decomposition". *IEEE Transactions on Geoscience and Remote Sensing*. Vol. 37.1999. pp. 1204 -1211.

10. R. Riyahi, C. Kleinn, H. Fuchs. "Comparison of Different Image Fusion Techniques for Individual Tree Crown Identification Using Quickbird Image". *International Society for Photogrammetry and Remote Sensing, High- Resolution Earth Imaging for Geospatial Information*. Vol. XXXVIII-1-4-7/W5. 2009. pp. 1-4.

11. Y. Zhang. "Understanding Image Fusion". *Photogrammetric Engineering & Remote Sensing*. Vol. 70. 2004. pp. 657-661.

12. L. Wald. "Some Terms of Reference in Data Fusion". *IEEE Trans Geoscience and. Remote Sensing*. Vol. 37. 1999. pp. 1190-1193.

13. MATLAB®. *Image Processing Toolbox User's Guide Vesion 2. For Use with MATLAB®*. 1998.

14. M. Misiti, Y. Misiti, G. Oppenheim, J. M. Poggi. *The Wavelet Toolbox. For Use MATLAB®*. 1996.

15. S. Mallat. "A Theory for Multiresolution Signal Decomposition: the Wavelet Representation". *IEEE Transactions on Pattern Analysis and Machine Intelligence*. Vol. 11. 1989. pp. 674-693.

16. I. Daubechies. "Orthonormal Basis of Compactly Supported Wavelets". *Communications on pure applied mathematics*. Vol. 41. 1988. pp. 909-996.

17. M. Gónzalez, X. Otazu, O. Fors, A. Seco. "Comparison Between Mallat's and the '*à* trous' Discrete Wavelet Transform Based Algorithms for the Fusion of Multispectral and Panchromatic Images". *IEEE Transactions on Geosciences and Remote Sensing*. Vol. 42. 2005. pp. 1291-1297.

18. Y. Nievergelt. *Wavelets made easy*. 1ª ed. Ed. Birkhäuser. Boston, USA. 1999. pp. 1-297.

19. I. Daubechies. *Ten Lectures on Wavelet*. 1ª ed. Ed. SIAM. Philadelphia, USA. 1992. pp.1-377.

20. S. Mallat. *A Wavelet Tour of Signal Processing*. 3ª ed. Ed. Elsevier. Philadelphia, USA. 2009. pp 1-832.

21. J. Jensen. *Introductory Digital Image Processing: A Remote Sensing Perspective*. 3rd ed. Ed. Prentice Hall. New Jersey, USA. 1996. pp. 1-554.

22. R. Medina, L. Joyanes, C. Pinilla. *Evaluación de la Transformada de Wavelet para Fusión de Imágenes Satelitales*. In conference record of 8th latin american and Caribbean conference for engineering and technology: innovation and development for the Americas: engineering, education, research and development. Arequipa, Perú. 2010. pp. 1-2.

23. R. Medina, L. Joyanes, C. Pinilla. Algoritmos Matemático para la Fusión de Imágenes Satelitales. In *V Simposio Internacional de Sistemas de Información e Ingeniería de Software en la Sociedad del Conocimiento*. 1ª ed. Ed. @LibroText. Bogotá Colombia. 2010. pp. 83-94.

24. S. Murray. *Estadística*. 2ª ed. Ed. Mc Graw Hill. Madrid, España. 1999. pp. 1-556

25. N. Otsu. "A Threshold Selection Method From Gray Level Histograms". *IEEE Transaction On Systems, Man and Cybernetics*. Vol. 9. 1979. pp. 62-66.

26. S. Al-Amri, N. Kalyankar, S. Khamitkar. "Image Segmentation by Threshold Techniques". *Journal of Computing*. Vol. 2. 2010. pp 83-87.

27. J. Cohen. "A Coefficient of Agreement for Nominal Scales". *Educational and Psychological Measurement*. Vol. 20. 1960. pp. 27-46.

28. R. Medina, I. Lizarazo. *Fusión de Imágenes Satelitales Usando la Transformada De Wavelet*. 1ª ed. Ed. Fondo de Publicaciones Universidad Distrital Francisco José de Caldas. Bogotá DC., Colombia. 2004. pp. 1-196.